Trap-State-Dominated Suppression of Electron Conduction in Carbon Nanotube Thin-Film Transistors

Qingkai Qian,[†,‡] Guanhong Li,[†,‡] Yuanhao Jin,[†,‡] Junku Liu,[†,‡] Yuan Zou,[†,‡] Kaili Jiang,[†,‡] Shoushan Fan,[†,‡] and Qunqing Li[†,‡,*]

[†]State Key Laboratory of Low-Dimensional Quantum Physics, Department of Physics & Tsinghua-Foxconn Nanotechnology Research Center, Tsinghua University, Beijing 100084, China and [‡]Collaborative Innovation Center of Quantum Matter, Beijing 100871, China

ABSTRACT The often observed p-type conduction of single carbon nanotube field-effect transistors is usually attributed to the Schottky barriers at the metal contacts induced by the work function differences or by the doping effect of the oxygen adsorption when carbon nanotubes are exposed to air, which cause the asymmetry between electron and hole injections. However, for carbon nanotube thin-film transistors, our contrast experiments between oxygen doping and electrostatic doping demonstrate that the doping-generated transport barriers do not introduce any observable suppression of electron conduction, which is further evidenced by the perfect linear behavior of transfer characteristics with the channel length scaling. On the basis of the above observation, we conclude that the environmental adsorbates work by more than simply shifting the Fermi level of the CNTs; more importantly, these adsorbates cause a poor gate modulation efficiency of electron conduction due to the relatively large trap state density near the conduction band edge of the carbon nanotubes, for which we further propose quantitatively that the adsorbed oxygen–water redox couple is responsible.

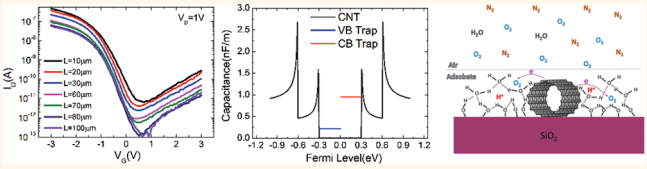

KEYWORDS: trap state · carbon nanotube · oxygen · redox · electrostatic

Carbon nanotubes (CNTs) are promising candidates for the next-generation electronic materials that possess exceptional properties such as large current-carrying capability[1] and outstanding carrier mobility.[2] For the real electronic application of CNT transistors, both p-type and n-type are needed to fabricate complementary metal-oxide-semiconductor circuits of high noise immunity and low static power consumption.[3] However, CNTs are very sensitive to the ambient environment, and the prepared transistors are often prone to exhibit p-type conduction;[4−7] thus the stable fabrication of n-type transistors has always been one of the major challenges for CNT transistors and great efforts have been made toward it. It has been reported that by using metals with different work functions as the source/drain, for example palladium or scandium, CNT field-effect transistors can be fabricated to be p-type or n-type.[8−11] Recent studies also suggest that n-type transistors can be created by the fixed positive charge at the interface between the SiO_2 substrate and ALD HfO_2[12,13] or by doping using low-work-function metal oxides.[14] Moreover, single carbon nanotube transistors with tunable polarities have been prepared by using a novel dual-gate structure to achieve a distinct p/i/p or n/i/n profile *via* electrostatic doping.[15]

To fabricate transistors with consistent and reproducible performance, studies on the mechanism of how the various factors determine the polarity of CNT transistors are essential. Considering the most typically observed p-type conduction of CNT field-effect transistors when exposed to air, recent studies have demonstrated that the hole doping is an electrochemical process mediated by the oxygen–water redox couple on the hydrophilic substrate,[16−18] which is also suggested to account for the recently observed Urbach tail in the effective density of states of carbon nanotubes.[19] Concerning how electron or hole conductions are further suppressed, up to now, most theories have been based on single CNT devices[4−6,9,15,20,21] and are focused on the Schottky barriers at the metal contacts, whether caused by work function

* Address correspondence to QunqLi@mail.tsinghua.edu.cn.

Received for review July 16, 2014 and accepted August 29, 2014.

Published online August 29, 2014
10.1021/nn503903y

differences or induced by the environmental doping effects,[4−6,9,21] except for the few cases of specially designed CNT devices with p/i/p or n/i/n profiles that can be explained like the similar conventional bulk transistors.[15,20]

However, for carbon nanotube thin-film transistors (TFTs), which are also often observed to be p-type when exposed to air,[22−24] whether the above barrier mechanisms still dominate should remain a question because the TFTs conduct through a percolation network that consists of many CNT junctions in addition to the metal contacts, which undoubtedly will reduce the significance of the Schottky barriers. Here, based on our designed experiments, we clearly demonstrate that the usual proposed doping-induced transport barriers (Schottky barriers or p−n junctions) do not dominate the p-type conduction of TFTs, which is further evidenced by the perfect linear performance of the transfer characteristics with channel length scaling. On the basis of the above observation, we conclude that the suppression of electron conduction is almost an intrinsic modulation behavior of CNTs when exposed to air, and it is the large trap state near the CNT conduction band edge that causes the poor subthreshold swing (SS) of electron conduction that results in the universal lack of n-type CNT TFTs when exposed to air. We further propose quantitatively that the adsorbed oxygen−water redox couple is responsible for these trap states.

RESULTS AND DISCUSSION

The carbon nanotubes we used were in powder form and purchased from NanoIntegris Inc. with a semiconductor purity of 98% and an average length of 1.8 μm, which were later dispersed in NMP (*N*-methyl-2-pyrrolidone, Sigma-Aldrich) with a CNT density of approximately 0.01 mg/mL. Devices were prepared on a 300 nm thermal SiO_2 on p^{++} Si substrate, and a schematic diagram of our fabricated TFTs is presented in Figure 1a. Twenty nanometers of different oxides were deposited as the gate dielectric separately, and we experimented with oxides such as e-beam-evaporated SiO_2 and ALD-deposited Al_2O_3 and HfO_2. Subsequently, CNTs were deposited on the oxides functionalized with aminopropyltriethoxysilane (APTES) by immersing into CNT solution, and the typical SEM image of the deposited CNT is shown in Figure 1b with a density of 5.4 $\mu m/\mu m^2$. The density of the CNTs is independent of the different dielectric oxides used. Then source−drain electrodes and interconnections between transistors were formed, and finally one additional photolithography together with oxygen plasma etching was used to define and isolate the active channel regions. The channel length and width of our fabricated devices are 48 and 40 μm, respectively; however, the gate length is only 44 μm. In other words, the 2 μm long channel regions near both the source and drain are out of modulation of the local gate.

The fabricated local-gated TFTs were measured using an Agilent 4156C semiconductor analyzer in the Lakeshore probe station, which could be pumped to a base pressure below 1×10^{-4} Pa and heated to 200 °C. The measured transfer characteristics of our devices with CNTs exposed to air are shown in Figure 1c; the source−drain voltage is set to 0.1 V, and the gate voltage is swept from −3 to 3 V. Despite different oxides such as SiO_2, Al_2O_3, and HfO_2 being used as the gate dielectrics, all the devices exhibit p-type conduction with electron conduction seriously suppressed as often reported, even though there are some slight differences between different oxides. Due to the relatively low density of the carbon nanotube thin film used and thus the small possibility of percolating of the CNT network through metallic carbon nanotubes,[25,26] all the transistors exhibit large on−off ratios as high as 10^5. In addition, the performances of devices with the same dielectric oxide display excellent consistency, which indicates high uniformity of the CNT films.

We further measured the same transistors in a vacuum; on the basis of previous reports, we knew that the vacuum itself could not desorb the molecules on the substrates.[5,6,12] Thus, we heated the samples to 180 °C for 2 h in a vacuum, and the transfer characteristics are shown in Figure 1d at V_D = 0.1 V. After eliminating the adsorbates, several changes occurred. First, all the devices changed to ambipolar conduction, with the minimum conduction voltages shifting left, which suggests that the adsorbates indeed account for the often observed p-type conduction. The minimum conduction voltages are different for the devices with different dielectrics, considering the transfer characteristics were measured by sweeping gate voltages from −3 to 3 V, which tends to make the minimum conduction voltages shift further left for transistors with larger hysteresis, so the minimum conduction voltage differences can be explained by the observed different hysteresis (not shown) of 0.60, 1.62, and 1.86 V for devices with SiO_2, Al_2O_3, and HfO_2 as dielectrics, respectively, which may result from the dielectrics themselves or the different hydrophilicity of the dielectric surfaces.[27] Finally, another striking change is the drastic decrease of the on-current for all the devices after baking in a vacuum by at least 2 orders of magnitude compared with the same measurements in air, which we believe is a sign of a large series resistance. Recalling that these devices are partially modulated by the local gate, we speculate that the large resistance results from the low carrier density of the 2 μm long channel outside the gate region.

To demonstrate the effect of the channel region outside the gate on the on-current, especially for the ambipolar transistors, we performed another

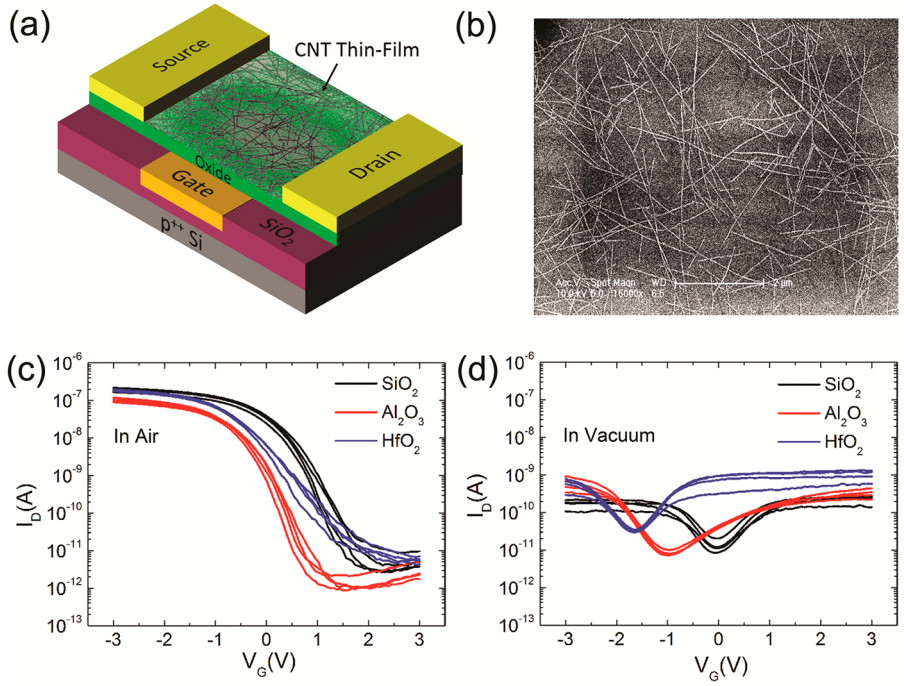

Figure 1. Performance of carbon nanotube TFTs in air and vacuum. (a) Schematic diagram of a local-gated TFT with gate embedded in the substrate (gate length L_g = 44 μm, channel length L = 48 μm, and channel width W = 40 μm). (b) SEM image of the carbon nanotube thin film with a typical density of 5.4 μm/μm^2. (c, d) Transfer characteristics of TFTs with 20 nm oxides (SiO_2, Al_2O_3, HfO_2 separately) as the dielectric measured at V_D = 0.1 V in air (c) and vacuum after baking at 180 °C for 2 h (d).

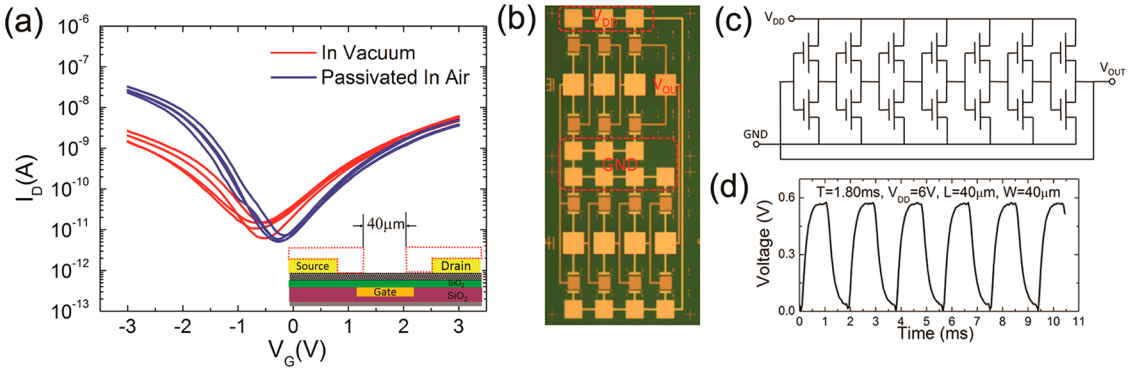

Figure 2. Effects of the partial modulation of the channel on the on-current and the time response of the ambipolar TFTs. (a) Transfer characteristics of TFTs with channel length shortened to L = 40 μm indicated by the dotted line in the inset schematic. In this plot, 20 nm SiO_2 is used as the dielectric, and the measurements were taken in a vacuum (red) and in air after passivation by ALD deposition of 20 nm Al_2O_3 (blue) at V_D = 0.1 V. (b) Optical microscopic image of a seven-stage ring oscillator. (c) Circuit diagram of the ring oscillator. (d) Output signal of the ring oscillator in a vacuum; the time delay of the inverter has decreased from 800 μs to 128 μs because of the shortened channel.

photolithography to reshape the active channel region with the channel length shortened to L = 40 μm by extending the source and drain as indicated by the dotted lines in the inset schematic of Figure 2a. The transfer characteristics were then remeasured in a vacuum after baking at 180 °C for 2 h, as represented by the red curves in Figure 2a, and the devices still exhibited ambipolar conduction. In addition, the on-current has increased significantly by at least 1 order of magnitude compared with that in Figure 1d for both hole and electron conduction, which undoubtedly supports our above speculation. The purpose of the above heating procedure in a vacuum was to eliminate the adsorbates on the substrate and the CNTs, which can also be fulfilled by the deposition of 20 nm ALD Al_2O_3, benefiting from the baking processing during the deposition and the relative compact structure of ALD to block the air.[12] The transfer characteristics after depositing 20 nm ALD Al_2O_3 still exhibit ambipolar conduction, as indicated by the blue curves in Figure 2a, even when the sample was later exposed to air. The increased on-current means less obstruction of carrier transport and thus faster time responses according to the intrinsic gate delay equation

$\tau_d = CV/I$.[28] To directly investigate this effect, we fabricated several seven-stage ring oscillators, for which an optical microscopic image and circuit diagram are presented in Figure 2b and c, respectively. The output oscillating signal after the channel length was shortened was measured in a vacuum, and the results are presented in Figure 2d. The delay time of each inverter decreased significantly from 800 μs to 128 μs after the channel length was shortened, which is mainly due to the increased on-current, indicating another key factor in fabricating carbon nanotube TFTs with higher speed beyond shortening the channel length and increasing the gate capacitance,[29] which is always maintaining the entire channel under gate modulation especially for the ambipolar transistors.

As observed in Figure 1c and d, the adsorbates of air on the TFTs can change the device performance drastically from ambipolar conduction to unipolar p-type; moreover, the on-current depends sensitively on the doping status of the channel regions outside the gate, as illustrated in Figure 2a. To further investigate the detailed effects of the air adsorptions, we measured the time-related gradual changes of the transfer characteristics immediately after breaking the vacuum and letting air enter the probe station for the same devices in Figure 1d. The measured transfer characteristics (V_D = 0.1 V) for a HfO_2 device are shown in Figure 3a, in which "Air 0 min" corresponds to a moment when the devices are totally exposed to air because the process of breaking the vacuum lasts several minutes, and to minimize the possible influence of hysteresis, the gate voltage is swept from −3 V to 3 V and back to −3 V again, but only the transfer characteristics swept from −3 V to 3 V are shown. During the 20 min after the introduction of air, the TFT gradually evolves from ambipolar conduction to p-type. The major changing tendencies are clearly indicated by arrows 1−3 in Figure 3a, which is always repeatable and also valid for devices with SiO_2 or Al_2O_3 as dielectrics. Specifically, first as indicated by arrow 1, the on-current of hole conduction increases with air exposure time, which is partly due to the shift of the Dirac point, as indicated by arrow 2, caused by the oxygen doping, but is mainly due to the increase of the carrier density in the 2 μm long channel regions outside the gate. Quite different from the increased hole conduction current, the electron conduction current decreases, as indicated by arrow 3, which changes the transfer characteristics asymmetrically from ambipolar to p-type.

The suppression of electron conduction when the devices are exposed to air has also been observed in single carbon nanotube field-effect transistors and is often attributed to the formation of Schottky barriers near the contacts caused by oxygen absorption.[4−6] Supposing that the barrier mechanism is also valid for our TFT devices, the asymmetry observed in Figure 3a should be the result of the formation of a p/n/p profile similar to that in the single-CNT cases,[15,20] because regions outside the gate are constantly doped to be p-type; thus even though the gate can modulate the middle channel part to n-type with a high electron density, the current should still be greatly suppressed because of the large resistance of the reverse-biased p−n junctions. To verify the possible current suppression effect of these p−n junctions, we attempted to establish the p/i/p or n/i/n profile simply by electrostatic doping. We began with the devices illustrated in Figure 1a with SiO_2 as the dielectric and deposited 20 nm of Al_2O_3 *via* ALD to eliminate the air adsorptions; then, the devices were measured using the embedded local gate with the substrate biased at different voltages as a global gate. The transfer characteristics are shown in Figure 3b; the voltages applied on the substrate are biased large enough to ensure a strong electrostatic doping. The results are quite astonishing: whether the channel is tuned to be a p/i/p or n/i/n profile by the substrate, no significant asymmetric suppressions of electron or hole conduction were observed, which overturns the assumption that the universal p-type carbon nanotube TFTs are caused simply by the oxygen-doping-induced barriers (p−n junctions).

In our above electrostatic doping case, the middle channel part is out of modulation of the substrate because of the screening effect of the embedded local gate; however, in the oxygen doping cases in Figure 3a, the entire channel is modulated by the air adsorptions. To clearly see the difference between oxygen doping and electrostatic doping without the involvement of the screening effect, we fabricated another device with a top gate to allow the entire channel to be modulated by the global back gate; the device structure is shown in Figure 3c, with 25 nm Al_2O_3 of ALD used as the top gate dielectric and to isolate the device from air. We performed the dual-gate measurement with the substrate biased again, and the results are presented in Figure 3d. By comparing the results with the performance of oxygen doping in Figure 3a, we can see that the substrate electrostatic doping increases the on-current of hole conduction and shifts the Dirac point by almost the same amount as oxygen doping; however, the substrate electrostatic doping does not introduce any observable asymmetries between electron and hole conductions, which is quite different from the oxygen doping. Moreover, by comparing arrow 2 in Figure 3a and d, we observe that the electrostatic doping shifts only the minimum conduction voltage; however, the oxygen doping also decreases the minimum current, which should be the effect of the charge impurity scattering by the adsorbates.[1,30,31] Above all, we conclude that the oxygen doping is playing roles more than simply shifting the Fermi level of the CNTs like electrostatic doping.

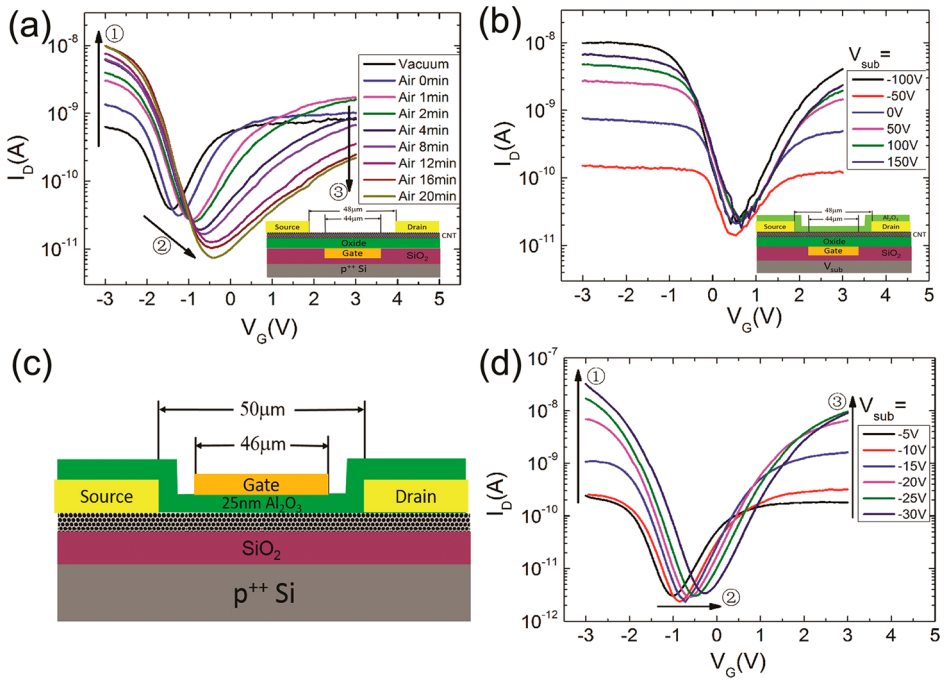

Figure 3. TFTs modulated by oxygen doping and electrostatic doping. (a) Local-gated transistor with 20 nm HfO_2 as the dielectric is first baked in a vacuum at 180 °C for 2 h, and then the transfer characteristics are measured at different times (~0, 1, 2, 4, 8, 12, 16, 20 min) after introducing air into the probe station chamber. (b) Transfer characteristics of the local-gated transistor with the highly p-doped substrate biased at different voltages; in this case, the oxygen is eliminated by ALD deposition of 20 nm Al_2O_3. (c, d) Schematic diagram and transfer characteristics of the top-gated transistor with the substrate biased at different voltages; the channel width is100 μm.

To obtain the carrier-determined intrinsic CNT conductance without the involvement of the effects of any possible Schottky barriers or p−n junctions, we used the transmission line method by fabricating embedded local-gated TFTs with scaling channel lengths varying from 10 to 100 μm; a 20 nm SiO_2 layer was used as the dielectric, the entire channel was modulated by the local gates, and the channel width was 100 μm. The measured transfer characteristics are shown in Figure 4a; the current decreases proportionally as the channel length increases, which indicates that no significant contact or junction resistances occur even when different gate voltages are applied. To quantitatively study this effect, we attempted to fit the device resistances to the different channel lengths under the same gate voltage, and the results are presented in Figure 4b. The black lines represent the fitted square resistances of the CNT film, and the red line represents the contact resistances with 100 μm width, shown together with their standard error bars; the blue curve represents the correlation coefficients, which indicate that the fittings are indeed all good linear fittings even when biased at different gate voltages. Thus, we observe that the contact or junction resistances are always ignorable when compared with the square resistances of the carbon nanotube thin film, even when the local gate is positive biased to form theoretically suggested relatively large barriers, and thus we conclude that the suppression of electron conduction in TFTs is almost an intrinsic dielectric modulation phenomenon when CNTs are exposed to air.

A logarithmic plot of the square resistances changing with the gate voltage is presented in Figure 4c, from which we can calculate the subthreshold swing (SS) for hole and electron conductions to be 303 mV/dec and 1.06 V/dec, respectively. Theoretically, the ideal SS can be as small as 60 mV/dec at room temperature; however, due to the presence of trap states in the band gap of CNTs, the measured SS deviates as $SS = (kT \ln(10)/e)(1 + (C_{it}/C_{ox}))$, where $C_{it} = e^2 N_{it}$ is the trap state capacitance, N_{it} is the trap state density, and C_{ox} is the dielectric capacitance. Because the carbon nanotube thin film we used is relatively sparse, the coupling capacitance of a single CNT can be calculated using $C_{ox} = (2\pi\varepsilon_0\varepsilon/\ln(2d/R)) = 5.4 \times 10^{-11}$ F/m,[32] where $\varepsilon = 3.9$ was used as the dielectric constant for SiO_2 and R = 0.7 nm was used as the average radius for our purchased CNTs; therefore, the trap state capacitance C_{it} near the valence band (VB) and conduction band (CB) can be calculated as 2.2×10^{-10} F/m and 9.5×10^{-10} F/m, respectively, which is comparable to the quantum capacitance $C_Q = 4 \times 10^{-10}$ F/m of an individual CNT.[33] To demonstrate this result more clearly, we schematically plot the density of states for the intrinsic CNT and the trap states in the band gap in Figure 4d, which suggests that it is the relatively larger trap state density near the conduction band that causes the asymmetry between the hole and electron conductions.

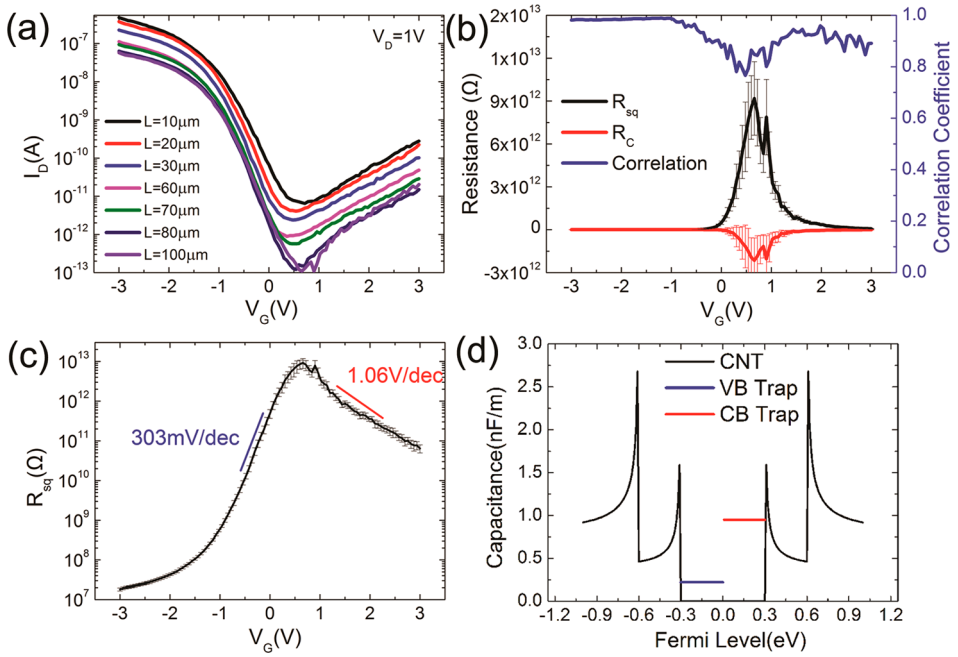

Figure 4. Length scaling of TFTs. (a) Transfer characteristics of TFTs with different channel lengths (10, 20, 30, 60, 70, 80, 100 μm) at V_D = 1 V; the channel width is 100 μm, and the entire channel is modulated by an embedded local gate through 20 nm evaporated SiO_2. (b) Linear fitting of the TFT resistance with channel length at different gate voltages. The fitted square resistances of the CNT film (black) and contact resistances (red) are plotted together with their standard error bars; the correlation coefficients (blue) indicate that these are indeed good linear fittings. (c) Logarithmic plot of CNT film square resistances at different gate voltages; the blue and red lines represent the subthreshold swings of the hole and electron conductions, respectively. (d) Density of the extracted charge trap states in the band-gap edges of the valence and conduction bands compared with the quantum capacitance of a single CNT.

Using the same method, we calculated the trap state densities of the same device, as shown in Figure 3a, at various times after breaking the vacuum, where we used ε = 20 as the dielectric constant for HfO_2.[34] The results are presented in Figure 5a; with the gradual air adsorption, the trap states near the conduction band (red) increase, while those near the valence band (blue) remain almost constant. It has been noted that the oxygen doping works by the mechanism of the oxygen–water redox couple, just as we schematically illustrate in Figure 5b,[16,17] in which the solvated oxygen in water sets the condition for the redox reaction $O_2(aq) + 4H^+ + 4e^- \underset{red}{\overset{ox}{\rightleftharpoons}} 2H_2O$. The included charge transfer process can be described by Marcus–Gerischer (MG) theory[35] as once demonstrated with graphene;[16] thus similarly, we plotted the energy diagram between the CNTs and oxygen–water redox couple system in Figure 5c, during which we used the oxygen concentration determined by Henry's law and pH = 6, the work function of the CNTs was set to 4.7 V,[36] and the band gap was set to 0.6 eV.[37] The Fermi level of the CNTs is higher than that of the oxygen–water redox couple; thus, the electrons will inject from the CNTs to the oxygen–water redox couple, causing the hole doping of CNTs.[17] However, we should note that the MG theory is designed to calculate the transient charge transfer, as indicated by the pink arrow in Figure 5c. When the system reaches equilibrium, the Fermi level of both the CNTs and the redox couple should be equal; in other words, $E_{F,CNT} = E_{F,redox}$, which can help us to obtain the final state of the redox system. In this case, the Fermi level of the redox couple is determined by[16]

$$E_{F,\,redox} = -5.71 - 0.0148[\log(C_{ox}) - 4\ pH] \quad (1)$$

where C_{ox} is the solved oxygen concentration (in units of mol/L) and pH is the acidity of the adsorbed water. On the other side, the total transferred charge can be calculated by

$$Q = eN_AV[c(OH^-) - c(H^+)] \quad (2)$$

where $N_A = 6.02 \times 10^{23}$ mol^{-1}, e is the elemental charge, and V is the volume of water involved. On the basis of eqs 1 and 2, the effective trap state density of the oxygen water redox couple can be calculated simply by

$$C_{it} = \frac{\partial Q}{\partial E_{F,\,redox}} \quad (3)$$

If the oxygen concentration is maintained saturated and constant as $C_{ox} = 2.7 \times 10^{-4}$ mol/L by Henry's law, the effective trap density can be calculated and is logarithmically plotted in Figure 5d, where we set the volume of water V to be 0.5 nm × 10 nm × 1 m, meaning if the thickness of adsorbed water is 0.5 nm,[16] the width of the involved water around the individual CNT is roughly estimated to be 10 nm in this charge transfer process, and the length of 1 m was selected for convenience to compare the trap density with the

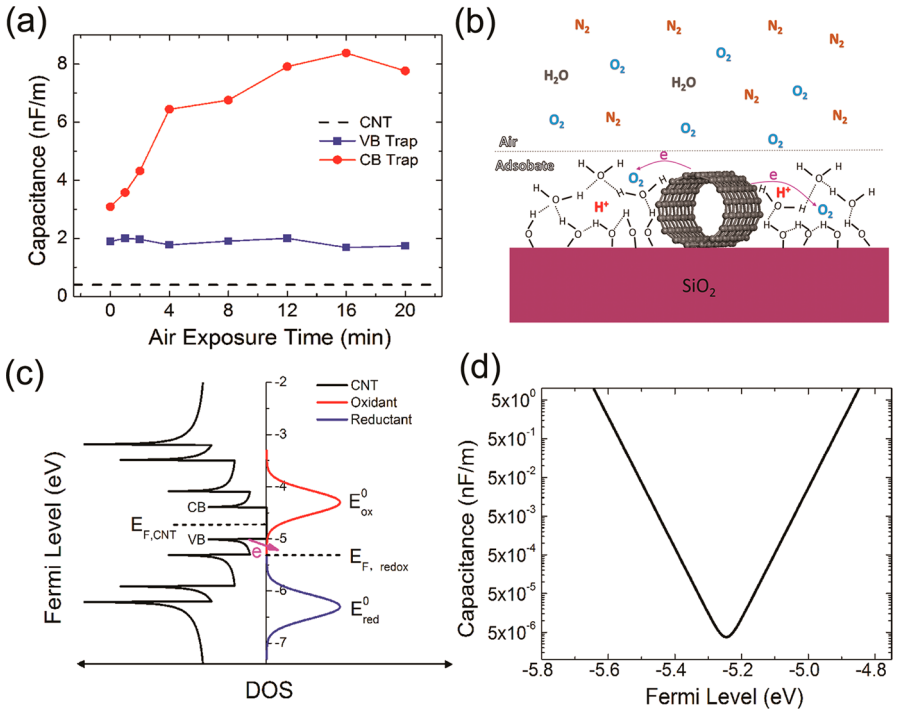

Figure 5. Effective trap state induced by the oxygen−water redox couple. (a) Trap state density extracted from Figure 3a evolves with air exposure time. (b) Schematic plot of the adsorbed oxygen−water redox couple and the charge transfer process with the CNT. (c) Energy diagram according to Marcus−Gerischer theory describing the transient charge transfer. (d) Effective capacitance of the trap state of the adsorbed oxygen−water redox couple.

quantum capacitance of an individual CNT. The effective density of states in the band-gap region of the CNT (−5.0 to −4.4 eV) is consistent with our experimental results and increases logarithmically by $\sim e^{E_F/kT}$, which corresponds precisely to the reported Urbach tail of the localized states observed by measuring the emission current after the gate pulse.[19] Our above model to calculate the effective trap state density should be only roughly correct because the real situation involves surface chemistry, and we have used solution chemistry as an approximation.

CONCLUSIONS

In summary, we have fabricated local-gated TFTs with different oxides as the dielectric, and all the devices exhibit similar p-type conduction when exposed to air and ambipolar conduction after baking in a vacuum, which indicates that the ambient adsorbates are responsible for the universal suppression of electron conduction. Considering that the hidden mechanism, especially for the TFT cases, is not clear, we performed detailed studies by designing some contrast experiments with electrostatic doping. Our results suggest that it is not the oxygen-doping-induced transport barriers (whether Schottky barriers or p−n junctions) that cause the suppression of electron conduction in TFTs, and the oxygen−water redox couple plays roles more than simply doping, and we suggest that it is their relatively larger trap state density near the conduction band edge of CNTs that results in the poor subthreshold swing of electron conduction that is responsible for the p-type conduction of CNT TFTs in air. Furthermore, we conjecture that the trap states of the water−oxygen redox couple should also work in the typical single CNT transistors when exposed to air, but how important these trap states are in determining the unipolar conduction compared with the usually proposed Schottky barriers requires further research.

METHODS

The carbon nanotubes we used were in powder form and purchased from NanoIntegris Inc., with a semiconductor purity of 98% and an average length of 1.8 μm, and were later dispersed in NMP (Sigma-Aldrich) using horn sonication with a CNT density of approximately 0.01 mg/mL. Devices were prepared on a 300 nm thermal SiO_2 on a p^{++} Si substrate. First, a standard photolithography was used to define the local gate, followed by reactive ion etching of 30 nm SiO_2 by CF_4, and the trenches were filled by e-beam evaporation of 5 nm Ti and 25 nm Pd as the embedded local gate. Then, 20 nm of different oxides were deposited as the gate dielectric separately, and we experimented with oxides such as e-beam-evaporated SiO_2 and ALD-deposited Al_2O_3 and HfO_2. Al_2O_3 was grown at 120 °C using trimethylaluminum (TMA) and water as the precursors, and HfO_2 was grown at 250 °C using tetrakis(dimethylamido)-hafnium ($Hf(NMe_2)_4$) and water as the precursors. Another photolithography and HF etch were used to form vial holes of the gates. To functionalize the oxide surface, we began with O_2 plasma etching to make it hydrophilic, and the samples were

immersed in an isopropyl alcohol (IPA)-diluted APTES (Sigma-Aldrich) solution (IPA:APTES = 1:20) for 30 min and then rinsed by IPA. Subsequently, the samples were immersed into the semiconducting nanotube solution for 6 min followed by a DI water rinse. After the deposition of the carbon nanotubes, the samples were annealed in a low-pressure oven with the mixed gases of 100 sccm Ar and 100 sccm H_2 at 400 °C for 1 h to drive off the solvent and other possible organic impurities. Then, 40 nm of Pd was evaporated to form source–drain electrodes and interconnections between transistors, and finally one additional photolithography together with oxygen plasma etching was used to define and isolate the active channel regions.

Conflict of Interest: The authors declare no competing financial interest.

Acknowledgment. This work was financially supported by the National Basic Research Program of China (2012CB932301) and the National Natural Science Foundation of China (90921012).

REFERENCES AND NOTES

1. Yao, Z.; Kane, C. L.; Dekker, C. High-Field Electrical Transport in Single-Wall Carbon Nanotubes. *Phys. Rev. Lett.* **2000**, *84*, 2941–2944.
2. Fuhrer, M. S.; Kim, B. M.; Dürkop, T.; Brintlinger, T. High-Mobility Nanotube Transistor Memory. *Nano Lett.* **2002**, *2*, 755–759.
3. Geier, M. L.; Prabhumirashi, P. L.; McMorrow, J. J.; Xu, W.; Seo, J. T.; Everaerts, K.; Kim, C. H.; Marks, T. J.; Hersam, M. C. Subnanowatt Carbon Nanotube Complementary Logic Enabled by Threshold Voltage Control. *Nano Lett.* **2013**, *13*, 4810–4814.
4. Martel, R.; Derycke, V.; Lavoie, C.; Appenzeller, J.; Chan, K.; Tersoff, J.; Avouris, P. Ambipolar Electrical Transport in Semiconducting Single-Wall Carbon Nanotubes. *Phys. Rev. Lett.* **2001**, 87.
5. Heinze, S.; Tersoff, J.; Martel, R.; Derycke, V.; Appenzeller, J.; Avouris, P. Carbon Nanotubes as Schottky Barrier Transistors. *Phys. Rev. Lett.* **2002**, 89.
6. Derycke, V.; Martel, R.; Appenzeller, J.; Avouris, P. Controlling Doping and Carrier Injection in Carbon Nanotube Transistors. *Appl. Phys. Lett.* **2002**, *80*, 2773.
7. Collins, P. G. Extreme Oxygen Sensitivity of Electronic Properties of Carbon Nanotubes. *Science* **2000**, *287*, 1801–1804.
8. Zhang, Z.; Wang, S.; Wang, Z.; Ding, L.; Pei, T.; Hu, Z.; Liang, X.; Chen, Q.; Li, Y.; Peng, L. Almost Perfectly Symmetric SWCNT-Based CMOS Devices and Scaling. *ACS Nano* **2009**, *3*, 3781–3787.
9. Zhang, Z.; Liang, X.; Wang, S.; Yao, K.; Hu, Y.; Zhu, Y.; Chen, Q.; Zhou, W.; Li, Y.; Yao, Y.; *et al.* Doping-Free Fabrication of Carbon Nanotube Based Ballistic CMOS Devices and Circuits. *Nano Lett.* **2007**, *7*, 3603–3607.
10. Shahrjerdi, D.; Franklin, A. D.; Oida, S.; Ott, J. A.; Tulevski, G. S.; Haensch, W. High-Performance Air-Stable n-Type Carbon Nanotube Transistors with Erbium Contacts. *ACS Nano* **2013**, *7*, 8303–8308.
11. Ding, L.; Wang, S.; Zhang, Z.; Zeng, Q.; Wang, Z.; Pei, T.; Yang, L.; Liang, X.; Shen, J.; Chen, Q.; *et al.* Y-Contacted High-Performance n-Type Single-Walled Carbon Nanotube Field-Effect Transistors: Scaling and Comparison with Sc-Contacted Devices. *Nano Lett.* **2009**, *9*, 4209–4214.
12. Zhang, J.; Wang, C.; Fu, Y.; Che, Y.; Zhou, C. Air-Stable Conversion of Separated Carbon Nanotube Thin-Film Transistors from p-Type to n-Type Using Atomic Layer Deposition of High-K Oxide and Its Application in CMOS Logic Circuits. *ACS Nano* **2011**, *5*, 3284–3292.
13. Moriyama, N.; Ohno, Y.; Kitamura, T.; Kishimoto, S.; Mizutani, T. Change in Carrier Type in High-K Gate Carbon Nanotube Field-Effect Transistors by Interface Fixed Charges. *Nanotechnol.* **2010**, *21*, 165201.
14. Suriyasena Liyanage, L.; Xu, X.; Pitner, G.; Bao, Z.; Wong, H. S. P. VLSI-Compatible Carbon Nanotube Doping Technique with Low Work-Function Metal Oxides. *Nano Lett.* **2014**, *14*, 1884–1890.
15. Lin, Y. M.; Appenzeller, J.; Knoch, J.; Avouris, P. High-Performance Carbon Nanotube Field-Effect Transistor with Tunable Polarities. *IEEE Trans. Nanotechnol.* **2005**, *4*, 481–489.
16. Levesque, P. L.; Sabri, S. S.; Aguirre, C. M.; Guillemette, J.; Siaj, M.; Desjardins, P.; Szkopek, T.; Martel, R. Probing Charge Transfer at Surfaces Using Graphene Transistors. *Nano Lett.* **2011**, *11*, 132–137.
17. Aguirre, C. M.; Levesque, P. L.; Paillet, M.; Lapointe, F.; St-Antoine, B. C.; Desjardins, P.; Martel, R. The Role of the Oxygen/Water Redox Couple in Suppressing Electron Conduction in Field-Effect Transistors. *Adv. Mater.* **2009**, *21*, 3087–3091.
18. Chakrapani, V.; Angus, J. C.; Anderson, A. B.; Wolter, S. D.; Stoner, B. R.; Sumanasekera, G. U. Charge Transfer Equilibria between Diamond and an Aqueous Oxygen Electrochemical Redox Couple. *Science* **2007**, *318*, 1424–1430.
19. Jones, D. A.; Lee, J. U. Observation of the Urbach Tail in the Effective Density of States in Carbon Nanotubes. *Nano Lett.* **2011**, *11*, 4176–4179.
20. Javey, A.; Tu, R.; Farmer, D. B.; Guo, J.; Gordon, R. G.; Dai, H. High Performance n-Type Carbon Nanotube Field-Effect Transistors with Chemically Doped Contacts. *Nano Lett.* **2005**, *5*, 345–348.
21. Moriyama, N.; Ohno, Y.; Suzuki, K.; Kishimoto, S.; Mizutani, T. High-Performance Top-Gate Carbon Nanotube Field-Effect Transistors and Complementary Metal–Oxide–Semiconductor Inverters Realized by Controlling Interface Charges. *Appl. Phys. Express* **2010**, *3*, 105102.
22. Wang, C.; Chien, J.; Takei, K.; Takahashi, T.; Nah, J.; Niknejad, A. M.; Javey, A. Extremely Bendable, High-Performance Integrated Circuits Using Semiconducting Carbon Nanotube Networks for Digital, Analog, and Radio-Frequency Applications. *Nano Lett.* **2012**, *12*, 1527–1533.
23. Wang, C.; Zhang, J.; Zhou, C. Macroelectronic Integrated Circuits Using High-Performance Separated Carbon Nanotube Thin-Film Transistors. *ACS Nano* **2010**, *4*, 7123–7132.
24. Sun, D.; Timmermans, M. Y.; Tian, Y.; Nasibulin, A. G.; Kauppinen, E. I.; Kishimoto, S.; Mizutani, T.; Ohno, Y. Flexible High-Performance Carbon Nanotube Integrated Circuits. *Nat. Nanotechnol.* **2011**, *6*, 156–161.
25. Hu, L.; Hecht, D. S.; Grüner, G. Percolation in Transparent and Conducting Carbon Nanotube Networks. *Nano Lett.* **2004**, *4*, 2513–2517.
26. Kumar, S.; Pimparkar, N.; Murthy, J. Y.; Alam, M. A. Theory of Transfer Characteristics of Nanotube Network Transistors. *Appl. Phys. Lett.* **2006**, *88*, 123505.
27. Kim, W.; Javey, A.; Vermesh, O.; Wang, Q.; Li, Y.; Dai, H. Hysteresis Caused by Water Molecules in Carbon Nanotube Field-Effect Transistors. *Nano Lett.* **2003**, *3*, 193–198.
28. Chau, R.; Datta, S.; Doczy, M.; Doyle, B.; Jin, B.; Kavalieros, J.; Majumdar, A.; Metz, M.; Radosavljevic, M. Benchmarking Nanotechnology for High-Performance and Low-Power Logic Transistor Applications. *IEEE Trans. Nanotechnol.* **2005**, *4*, 153–158.
29. Ha, M.; Seo, J. T.; Prabhumirashi, P. L.; Zhang, W.; Geier, M. L.; Renn, M. J.; Kim, C. H.; Hersam, M. C.; Frisbie, C. D. Aerosol Jet Printed, Low Voltage, Electrolyte Gated Carbon Nanotube Ring Oscillators with Sub-5 μs Stage Delays. *Nano Lett.* **2013**, *13*, 954–960.
30. Chen, J. H.; Jang, C.; Adam, S.; Fuhrer, M. S.; Williams, E. D.; Ishigami, M. Charged-Impurity Scattering in Graphene. *Nat. Phys.* **2008**, *4*, 377–381.
31. Nakanishi, T.; Tsuneya, A. Numerical Study of Impurity Scattering in Carbon Nanotubes. *J. Phys. Soc. Jpn.* **1999**, *68*, 561–566.
32. Cao, Q.; Xia, M.; Kocabas, C.; Shim, M.; Rogers, J. A.; Rotkin, S. V. Gate Capacitance Coupling of Singled-Walled Carbon Nanotube Thin-Film Transistors. *Appl. Phys. Lett.* **2007**, *90*, 23516.
33. Rosenblatt, S.; Yaish, Y.; Park, J.; Gore, J.; Sazonova, V.; McEuen, P. L. High Performance Electrolyte Gated Carbon Nanotube Transistors. *Nano Lett.* **2002**, *2*, 869–872.

34. Javey, A.; Guo, J.; Farmer, D. B.; Wang, Q.; Wang, D.; Gordon, R. G.; Lundstrom, M.; Dai, H. Carbon Nanotube Field-Effect Transistors with Integrated Ohmic Contacts and High-K Gate Dielectrics. *Nano Lett.* **2004**, *4*, 447–450.
35. Memming, R. Electron Transfer Theories. In *Semiconductor Electrochemistry*; Wiley-VCH: Weinheim, 2001; pp 112−150.
36. Liu, P.; Sun, Q.; Zhu, F.; Liu, K.; Jiang, K.; Liu, L.; Li, Q.; Fan, S. Measuring the Work Function of Carbon Nanotubes with Thermionic Method. *Nano Lett.* **2008**, *8*, 647–651.
37. Ouyang, M.; Huang, J.; Lieber, C. M. Fundamental Electronic Properties and Applications of Single-Walled Carbon Nanotubes. *Acc. Chem. Res.* **2002**, *35*, 1018–1025.